Heuristic imaging from generic projections : backprojection outside the range of the Radon transform

Jean-Baptiste Bellet, Gérard Berginc

HEURISTIC IMAGING FROM GENERIC PROJECTIONS: BACKPROJECTION OUTSIDE THE RANGE OF THE RADON TRANSFORM

JEAN-BAPTISTE BELLET AND GÉRARD BERGINC

Abstract. Reflective tomography is an efficient method for optical imaging in the visible and near infrared ranges. It computes empirical reconstructions based on algorithms from X-ray tomography. This subject introduces mathematical gaps to be filled, about the meaning of the reconstructions, and about their artifacts. To tackle these questions, we study more generally the filtered backprojection on projections outside the range of the Radon transform. We consider generic projections that can involve any kind of physical and geometric parameters. We claim that the backprojection contains partially the geometry of the original scene. More precisely, we compare the singularities of the backprojection with the singularities of a representation of the scene. This comparison of wavefront sets, inspired by studies of the artifacts in X-ray tomography, is based on microlocal analysis. It gives a precise meaning to the well-reconstructed geometry, describes the invisible parts, and the artifacts. We illustrate the heuristic and the analysis principle on canonical cases that belong to various fields: shape from silhouettes, constructible tomography, cloaking, reconstruction from cartoon images, imaging of occluded lambertian objects. Numerical results show the relevance of the heuristic and its analysis. In a word, this study provides a mathematical framework that covers the solver of reflective tomography, and exhibits an imaging method whose range of application is wide.

1. Introduction

1.1. **Tomography.** In usual tomography, the practitioners measure the attenuation of X-rays through a medium. Then the records are processed to provide a reconstruction of a spatial function, representing the attenuation property of the materials. From a mathematical point of view, the measurements are line integrals of the attenuation function: they contain information about the X-ray transform of a fixed function, or the Radon transform in two dimensions. So the reconstruction method looks like a Radon inversion, or an X-ray inversion, which is often implemented using analytical formulas such as the filtered backprojection algorithm. This is the basis of transmission tomography and it is a well known subject [10].

The Radon transform has also been studied in a framework of microlocal analysis [11]: it is a Fourier Integral Operator. In particular there are correspondences between the singularities of a distribution and the singularities of its Radon transform. This is for example the basis of geometrical tomography [12] where the singularities of an attenuation are reconstructed from the singularities of its Radon transform. Furthermore this provides a framework for the description of artifacts that arise from limited data in transmission tomography [3, 5].

1.2. **Reflective tomography.** The efficiency of the filtered backprojection leaded several authors to use the method, outside the framework of X-ray inversion, for other ranges of wavelengths. We have especially in mind the so-called *reflective tomography*, in the visible-near infrared band. This subject emerged at the end of the 80's in the context of laser radar imaging [8], and has been introduced in other frameworks, such as modeling from photographs [6] and three-dimensional optronic identification [1, 2]. The common principle of these heuristic methods: assuming that the measurements contain *reflective* projections of a scene, compute a reconstruction by the means of a tomographic algorithm. It is observed in numerical experiments that the peaks of such reconstructions provide the well-reconstructed parts of the original surfaces, up to artifacts.

Date: September 16, 2019.

2000 *Mathematics Subject Classification.* 78A97, 94A12, 44A12.

Key words and phrases. 3D imaging, computational optics, reconstruction, Radon transform, geometric tomography.

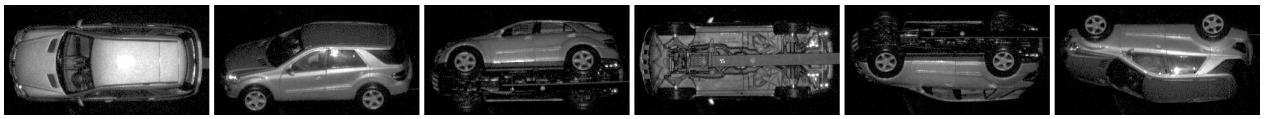

FIGURE 1. A few images of a sequence of 2D real images in the visible-near infrared band.

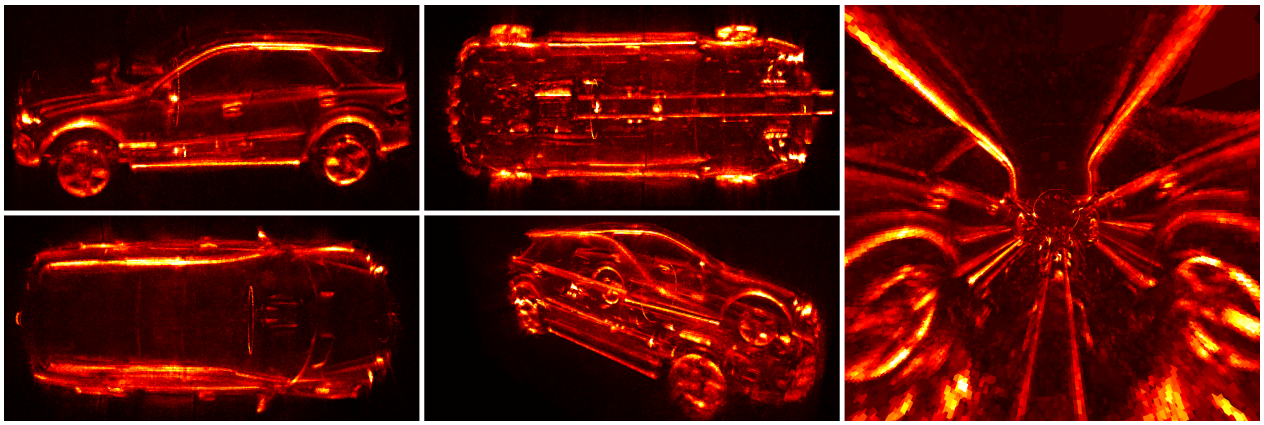

FIGURE 2. Volume rendering of a 3D tomographic reconstruction from real 2D optical images.

1.3. **Optical imaging based on reflective tomography: example.** The following real example illustrates the efficiency of reflective tomography in three-dimensional optical imaging. We consider a sequence of 360 images of size 342×181, measured by turning around the scene, one degree step. These active images have been recorded in the visible-near infrared band (courtesy of Thales Optronique SA). See Figure 1 for samples of the sequence. Using a home-made software, the tomographic reconstruction from these 360 images takes 2.6 seconds on a Graphics Processing Unit (Nvidia Tesla C2075). Then the reconstruction is displayed in real-time, using a volume rendering method. The Maximum Intensity Projection is very efficient: it selects the peaks. In the Figure 2, we represent snapshots of such re-projections. It is clear that reflective tomography is relevant: the reconstruction contains surfaces of the original scene with many features and details.

1.4. **Backprojection outside the range of the transform.** Nevertheless reflective tomography is only a heuristic method. There is indeed no guarantee that a reflective dataset belongs to the range of the X-ray transform. Thus there is a question about the meaning of a tomographic reconstruction from such data. Furthermore many materials are opaque for optical wavelengths. This is a major difference with X-ray wavelengths and has a strong consequence: in general there are occlusions. The superposition principle is violated and so the optical projection cannot be modeled by the X-ray transform, and we come back to the question about the meaning. Moreover the occlusions introduce incompleteness in the data [13], while it is known in the field of transmission tomography that incompleteness introduces artifacts in the reconstruction [3]. Other questions arise, concerning the artifacts of reflective tomography, and especially concerning the artifacts due to the occlusions.

1.5. **Contributions of this work.**

1.5.1. *Framework of a generic imaging method.* This work extends the principle of reflective tomography: it motivates the use of the Radon backprojection outside the range of the Radon transform. Such a generic principle provides an efficient heuristic for inverse problems involving projections along rays: the filtered backprojection. The forward model describing the dataset can be linear or nonlinear; it can depend on physical properties and on geometric properties. The principle can be applied without precising the forward

model, similarly as the gradient detects contours in image processing, without modeling the process of image formation. Furthermore the dataset can be complete or incomplete.

The heuristic process computes a reconstruction that represents the projected scene. We focus on the geometry of the reconstruction: we select the wavefront set as a relevant information. In this way we give a precise meaning to a filtered backprojection outside the range of the Radon transform: it must be understood that the method aims at computing a function whose wavefront set represents the geometry of the original scene.

Moreover we propose a framework to analyze the heuristic. The key point is to compare the wavefront set of the reconstruction with the wavefront set of a reference model of the scene, taking benefit from the canonical relations of the Radon transform and its dual. We write, in the spirit of [3], and in a generic way: the well-reconstructed parts, the invisible parts and the artifacts. In particular we show circumstances where singularities of the dataset disappear during the backprojection; such situations never happen in transmission tomography, but in a general setting, it can happen with anti-symmetry properties.

1.5.2. *Study of canonical cases.* We apply and analyze the heuristic on canonical cases corresponding to various kinds of projections.

We consider model problems with silhouettes, where we have to deal with smooth sets, occlusions, corners and edges. We obtain the following results. A smooth convex set is recovered. A convex polygon is recovered with artifacts: the lines containing the sides. For two smooth convex sets, the nonlinearity due do the occlusions is translated under the form of a product. Then the sets are only partially recovered, and corners of the dataset generate artifacts along the common tangents of the initial sets.

We show two original applications. An example of constructible tomography where the heuristic recovers exactly the singularities of a constructible function from its constructible Radon transform [14]. And we construct a case where a kind of cloaking is achieved: the object is visible in the projections but completely disappears during the backprojection. Then we show that breaking the anti-symmetry counters this effect.

Furthermore we study the case of two smooth convex sets projected under the form of contrasted cartoon images. We decompose the dataset by the means of operations on silhouettes. This is a way to deal with the concealment. More particularly the concealment interactions between the objects appear as the product of the individual silhouettes. We show that in comparison with the silhouettes, the wavefront set of the cartoon images is larger. This enables the full reconstruction of the two convex sets, while the occlusions produce the same kind of artifacts.

To finish with we model a case of reflective tomography, with two lambertian disks. We show that the structure of this problem is essentially the same than the cartoon one: the projections look like cartoon images weighted by a smooth factor depending on the geometry. In particular the Radon inversion is expected to reconstruct the circles, with the common tangent as artifacts. To the authors' knowledge, this is the first time that such a rigorous result is derived in reflective tomography: we have proposed a rigorous meaning for the reconstruction (the wavefront set), we have shown how to deal with the nonlinearity of the occlusions (product of silhouettes), we have estimated the well-reconstructed parts and the artifacts.

1.6. **Organization.** The paper is organized as follows. We formulate a generic principle of imaging, and we compare the wavefront set of such a reconstruction with the wavefront set of a representation of the scene. Then we apply the principle on various cases; in particular we illustrate the artifacts due to truncation, and we study nonlinearities due to concealment. The approach is strengthened by numerical experiments. This paper takes benefit from known results about microlocal analysis of the Radon transform, summarized in the appendix.

2. Imaging of singularities

2.1. Heuristic method.

Heuristic. *Let $g \in L^1_{\mathrm{loc}}([0,2\pi]\times\mathbb{R})$ be a generic function. We assume that $g(\theta,s)$ represents a kind of projection of a scene, along the ray $L(\theta,s) : x\cdot\boldsymbol{\theta} = s$. In order to recover the scene, we introduce the dual of the Radon transform $\mathcal{R}^*$, and we fix a pseudodifferential operator Λ. Then we consider that the filtered backprojection $\mathcal{R}^*\Lambda g$ is a representation of the original scene. More precisely, we claim that if $f \in L^2(\mathbb{R}^2)$ represents the scene, then the heuristic reconstruction $\mathcal{R}^*\Lambda g$ should have similarities with f.*

2.1.1. *Transmission tomography.* To illustrate the principle, we mention several known cases of imaging that enters in this framework, in transmission tomography. The first one is the natural one: $g = \mathcal{R}f$ is a Radon transform. In that case, we set $\Lambda = \frac{1}{4\pi}\sqrt{-\partial_s^2}$, and then we have exactly $\mathcal{R}^*\Lambda g = f$. With the same data $g = \mathcal{R}f$, in local tomography [4], we set $\Lambda = -\partial_s^2$, and then $\mathrm{WF}\,\mathcal{R}^*\Lambda g = \mathrm{WF}\,f$: in that case, the similarities of $\mathcal{R}^*\Lambda g$ and f are the wavefront sets. Furthermore, for limited data, $g = \mathbb{1}_A\mathcal{R}f$, where $A \subset [0,2\pi]\times\mathbb{R}$ defines the set of rays for which the Radon transform is known. In that case, with the usual filter $\Lambda = \frac{1}{4\pi}\sqrt{-\partial_s^2}$, the wavefront set $\mathrm{WF}\,\mathcal{R}^*\Lambda g$ captures partially the wavefront set of $\mathrm{WF}\,f$, and is augmented by a set which defines artifacts [3].

2.1.2. *Original applications.* As we will do in the next section, the principle covers original applications in other fields than transmission tomography. In a generic way, g comes from measurements depending on physical parameters and on geometric quantities.

2.2. Mathematical framework.

We propose a framework to analyze such a heuristic, in the spirit of [3]. The analysis is based on the canonical relations of the Radon transform: see Appendix A. The scheme is the following. We assume that the scene is represented by $f \in L^2(\mathbb{R}^2)$. In order to investigate the similarities between the reconstruction $\mathcal{R}^*\Lambda g$ and f, we focus on the singularities: we compare the wavefront sets $\mathrm{WF}(\mathcal{R}^*g)$ and $\mathrm{WF}(f)$. To do this, we start by comparing $\mathrm{WF}(g)$ with $\mathrm{WF}(\mathcal{R}f)$, where there is a correspondence between $\mathrm{WF}(\mathcal{R}f)$ and $\mathrm{WF}(f)$ due to the canonical relation (15) of $\mathcal{R}$. Then we deduce links between $\mathrm{WF}(\mathcal{R}^*g)$ and $\mathrm{WF}(f)$ from the canonical relation (18) of $\mathcal{R}^*$.

Proposition 1 (Correct reconstruction versus artifacts)**.** *Let $g \in L^1_{\mathrm{loc}}([0,2\pi]\times\mathbb{R})$, and $f \in L^2(\mathbb{R}^2)$. We set:*

$$\check{C}(g,f) := \mathrm{WF}(g)\cap\mathrm{WF}(\mathcal{R}f), \quad C(g,f) := \big\{(s\boldsymbol{\theta} - \frac{\hat\theta}{\sigma}\boldsymbol{\theta}^\perp, \sigma\boldsymbol{\theta}) : (\theta,s,\hat\theta,\sigma) \in \check{C}(g,f), \sigma\neq 0\big\},$$

$$\check{A}(g,f) := \mathrm{WF}(g)\setminus\mathrm{WF}(\mathcal{R}f), \quad A(g,f) := \big\{(s\boldsymbol{\theta} - \frac{\hat\theta}{\sigma}\boldsymbol{\theta}^\perp, \sigma\boldsymbol{\theta}) : (\theta,s,\hat\theta,\sigma) \in \check{A}(g,f), \sigma\neq 0\big\}.$$

(i) The wavefront set $\mathrm{WF}(g)$ is the disjoint union $\mathrm{WF}(g) = \check{C}(g,f)\cup\check{A}(g,f)$, and

$$\mathrm{WF}(\mathcal{R}^*g) \subset C(g,f)\cup A(g,f). \tag{1}$$

Furthermore, if g satisfies the symmetry property $g(\theta+\pi,-s) = g(\theta,s)$, then $\mathrm{WF}(\mathcal{R}^*g) = C(g,f)\cup A(g,f)$.
(ii) The wavefront set of f satisfies:

$$C(g,f) \subset \mathrm{WF}(f), \quad A(g,f)\cap\mathrm{WF}(f) = \emptyset. \tag{2}$$

Proof. (i) is exactly the canonical relation (18) of $\mathcal{R}^*$, while (ii) is a consequence of the canonical relation (15). □

The set $\check{C}(g,f)$ contains the singularities of g that are also singularities of $\mathcal{R}f$. After backprojection, this set provides a subset of the singularities of f: $\mathrm{WF}(\mathcal{R}^*g)\cap C(g,f) \subset \mathrm{WF}(f)$. As a result, the set of singularities $\mathrm{WF}(\mathcal{R}^*g)\cap C(g,f)$ defines correct similarities between the heuristic reconstruction $\mathcal{R}^*g$ and the representation f of the scene. The set $\check{A}(g,f)$ contains the other singularities of g. After backprojection, it produces singularities that are not singularities of the representation f: $A(g,f)\cap\mathrm{WF}(f) = \emptyset$. Thus, if we focus on the wavefront sets, the set of singularities $\mathrm{WF}(\mathcal{R}^*g)\cap A(g,f)$ corresponds to the artifacts of reconstruction.

Proposition 2 (Invisibility). *Let $g \in L^1_{\mathrm{loc}}([0,2\pi]\times\mathbb{R})$, and $f \in L^2(\mathbb{R}^2)$. We set:*

$$\check{I}(g,f) := \mathrm{WF}(\mathcal{R}f) \setminus \mathrm{WF}(g),$$
$$I(g,f) := \big\{(s\boldsymbol{\theta} - \frac{\hat\theta}{\sigma}\boldsymbol{\theta}^\perp, \sigma\boldsymbol{\theta}) : (\theta,s,\hat\theta,\sigma) \in \check{I}(g,f), (\theta+\pi,-s,\hat\theta,-\sigma) \in \check{I}(g,f), \sigma\neq 0\big\}.$$

Then

$$\mathrm{WF}(f) = C(g,f) \cup I(g,f), \quad C(g,f)\cap I(g,f) = \emptyset. \tag{3}$$

Proof. We get from (16): $\mathrm{WF}\, f = C(g,f)\cup J$, with

$$J = \big\{(s\boldsymbol{\theta} - \frac{\hat\theta}{\sigma}\boldsymbol{\theta}^\perp, \sigma\boldsymbol{\theta}) : (\theta,s,\hat\theta,\sigma) \in \check{I}(g,f), \sigma\neq 0\big\}.$$

We have $I(g,f)\subset J$, and we check that $J\setminus I(g,f)\subset C(g,f)$: if $(x,\hat x)\in J\setminus I(g,f)$, $\exists(\theta,s,\hat\theta,\hat s)\in\check{I}(g,f), \exists\sigma\neq 0, \Phi(x,\hat x,\theta,s,\hat\theta,\hat s,\sigma)=0$, with $(\theta+\pi,-s,\hat\theta,-\hat s)\notin\check{I}(g,f)$. Then $\Phi(x,\hat x,\theta+\pi,-s,\hat\theta,-\hat s)=0$, and then we get from (15): $(\theta+\pi,-s,\hat\theta,-\hat s)\in \mathrm{WF}\,\mathcal{R}f\cap\mathrm{WF}\, g$; therefore $(x,\hat x)\in C(g,f)$. □

The set $\check{I}(g,f)$ contains the singularities of $\mathcal{R}f$ that are not singularities of g. After backprojection, $I(g,f)$ contains the singularities of f that are invisible in g: they are not reconstructed due to $\mathrm{WF}(\mathcal{R}^*g)\cap C(g,f)\cap I(g,f)=\emptyset$.

Lemma 1. *Let $g\in L^1_{\mathrm{loc}}([0,2\pi]\times\mathbb{R})$. We define the symmetric part of g as*

$$g_{\mathrm{sym}}(\theta,s) = \frac{1}{2}(g(\theta,s)+g(\theta+\pi,-s)).$$

Then $\mathcal{R}^*g = \mathcal{R}^*g_{\mathrm{sym}}$.

Proof. By a simple calculus (change of variable $\theta := \theta-\pi$) we see that $\mathcal{R}^*[g(\theta+\pi,-s)](x) = \mathcal{R}^*[g](x)$. □

Due to this lemma, it is sufficient to study the reconstruction from the symmetric part g_{sym} of g.

Proposition 3 (Disappearance). *Let $g\in L^1_{\mathrm{loc}}([0,2\pi]\times\mathbb{R})$, and $f\in L^2(\mathbb{R}^2)$. We set:*

$$D(g,f) := C(g,f)\setminus \mathrm{WF}(\mathcal{R}^*g).$$

(i) If g is symmetric, i.e. *$g(\theta,s)=g(\theta+\pi,-s)$, then*

$$D(g,f)=\emptyset. \tag{4}$$

(ii) More generally:

$$D(g,f) = \big\{(s\boldsymbol{\theta} - \frac{\hat\theta}{\sigma}\boldsymbol{\theta}^\perp, \sigma\boldsymbol{\theta}) : (\theta,s,\hat\theta,\sigma) \in \mathrm{WF}(g)\cap\mathrm{WF}(\mathcal{R}f)\setminus\mathrm{WF}(g_{\mathrm{sym}}), \sigma\neq 0\big\}. \tag{5}$$

Proof. (i) If g is symmetric then (18) is an equality and so $\mathrm{WF}(\mathcal{R}^*g) = C(g,f)\cup A(g,f)\supset C(g,f)$.
(ii) Due to $\mathcal{R}^*g=\mathcal{R}^*g_{\mathrm{sym}}$: $D(g,f) = C(g,f)\setminus\mathrm{WF}(\mathcal{R}^*g_{\mathrm{sym}}) = C(g,f)\setminus C(g_{\mathrm{sym}},f)$. □

The set $D(g,f)$ represents the singularities of f that are not reconstructed by the heuristic $\mathcal{R}^*g$, while the dataset g contains the corresponding singularities of $\mathcal{R}f$: they disappear during the backprojection. In transmission tomography, this set is always empty (case (i)) due to the symmetry $g(\theta,s)=g(\theta+\pi,-s)$: the backprojection cannot kill any singularities. But more generally, it is possible that $D(g,f)\neq\emptyset$: the case (ii) states that a correct singularity of g, $(\theta_0,s_0,\hat\theta,\sigma)\in C(g,f)$, disappears during the backprojection if, and only if, the symmetric part g_{sym} is smooth at $(\theta_0,s_0,\hat\theta,\sigma)$: this a kind of "anti-symmetry" that means that $g(\theta+\pi,-s)$ and $g(\theta,s)$ are opposite in a neighborhood of (θ_0,s_0), up to a function smooth in the direction $(\hat\theta,\sigma)$.

2.3. **Synthesis.** Finally, when a method based on the heuristic principle is derived, eventually for g outside the range of the Radon transform, we propose to give a meaning to the heuristic reconstruction $\mathcal{R}^*g$, based on the wavefront set. In that case, the following disjoint unions must be investigated:

$$\begin{aligned} \mathrm{WF}\, f &= [\mathrm{WF}\, \mathcal{R}^*g \cap C(g,f)] \cup D(g,f) \cup I(g,f), \\ \mathrm{WF}\, \mathcal{R}^*g &\subset C(g,f) \cup A(g,f). \end{aligned}$$

In particular, they describe the well-reconstructed parts and the artifacts.

3. Applications

We test the imaging principle on various canonical examples. These examples involve silhouettes and so we start by formulating some rules of calculus with silhouettes.

3.1. **Computing with silhouettes.** Let $K \subset \mathbb{R}^2$ be a compact set such that: $K \neq \emptyset$ and $\overline{\mathrm{int}\, K} = K$. Along the line $L(\theta, s)$, the silhouette of K is defined by:

$$\mathcal{S}[K](\theta,s) := \begin{cases} 1, & \text{if } L(\theta,s) \cap K \neq \emptyset, \\ 0 & \text{otherwise,} \end{cases} \qquad \theta \in [0,2\pi], s \in \mathbb{R}. \tag{6}$$

We formulate preliminary results concerning the effect of some operations on the wavefront sets of silhouettes.

3.1.1. *Sum or counter.* The sum of silhouettes $\mathcal{S}[K_1] + \mathcal{S}[K_2]$ counts the number of objects K_1 and K_2 encountered along the ray of projection:

$$\mathcal{S}[K_1](\theta,s) + \mathcal{S}[K_2](\theta,s) = \begin{cases} 0, & \text{if } L(\theta,s) \cap (K_1 \cup K_2) = \emptyset, \\ 2, & \text{if } L(\theta,s) \cap K_1 \neq \emptyset \text{ and } L(\theta,s) \cap K_2 \neq \emptyset, \\ 1, & \text{otherwise.} \end{cases} \qquad \theta \in [0,2\pi], s \in \mathbb{R}.$$

The wavefront set of the sum is included in the union of the wavefront sets:

$$\mathrm{WF}\, \mathcal{S}[K_1] + \mathcal{S}[K_2] \subset \mathrm{WF}\, \mathcal{S}[K_1] \cup \mathrm{WF}\, \mathcal{S}[K_2], \text{ with equality if } \mathrm{WF}\, \mathcal{S}[K_1] \cap \mathrm{WF}\, \mathcal{S}[K_2] = \emptyset. \tag{7}$$

3.1.2. *Product or occlusion.* The product of silhouettes $\mathcal{S}[K_1]\mathcal{S}[K_2]$ takes the value 1 for the rays that intersects both K_1 and K_2, and 0 otherwise. This product represents a property of concealment; $\mathcal{S}[K_1]\mathcal{S}[K_2](\theta,s) = 1$ means: along the ray $L(\theta,s)$, K_1 conceals K_2 or K_2 conceals K_1. Assuming that

$$(\theta,s,\hat\theta,\hat s) \in \mathrm{WF}\, \mathcal{S}[K_1] \Rightarrow (\theta,s,-\hat\theta,-\hat s) \notin \mathrm{WF}\, \mathcal{S}[K_2], \tag{8}$$

then the product $\mathcal{S}[K_1]\mathcal{S}[K_2]$ satisfies [7]:

$$\mathrm{WF}\, \mathcal{S}[K_1]\mathcal{S}[K_2] \subset \{(\theta,s,\hat\theta_1+\hat\theta_2,\hat s_1+\hat s_2) : (\theta,s,\hat\theta_i,\hat s_i) \in \mathrm{WF}\, \mathcal{S}[K_i] \cup \mathrm{supp}\, \mathcal{S}[K_i] \times \{0\}, i=1,2\}; \tag{9}$$

here $\mathrm{supp}\, \mathcal{S}[K_i] = \{(\theta,s) : L(\theta,s) \cap K_i \neq \emptyset\}$ represents the set of rays that intersect K_i.

3.1.3. *Union.* The silhouette of a union satisfies $\mathcal{S}[K_1 \cup K_2] = 1 - (1 - \mathcal{S}[K_1])(1 - \mathcal{S}[K_2])$: it takes the value 1 on (θ,s) if, and only if, $L(\theta,s)$ intersects at least one of the K_i. Assuming (8) then

$$\begin{aligned} \{(\theta,s,\hat\theta,\hat s) \in \mathrm{WF}\, \mathcal{S}[K_i] : (\theta,s) \in \mathrm{supp}(1-\mathcal{S}[K_{\bar\imath}]), i=1,2\} &\subset \mathrm{WF}\, \mathcal{S}[K_1 \cup K_2] \\ &\subset \{(\theta,s,\hat\theta_1+\hat\theta_2,\hat s_1+\hat s_2) : (\theta,s,\hat\theta_i,\hat s_i) \in \mathrm{WF}\, \mathcal{S}[K_i] \cup \mathrm{supp}(1-\mathcal{S}[K_i]) \times \{0\}, i=1,2\}; \end{aligned} \tag{10}$$

here, $\mathrm{supp}(1 - \mathcal{S}[K_i]) = \{(\theta,s) : L(\theta,s) \cap \mathrm{int}\, K_i = \emptyset\}$ is the set of rays that do not penetrate inside K_i and $K_{\bar\imath} = K_1 \cup K_2 \setminus K_i$ $(\bar\imath = i + 1(2))$.

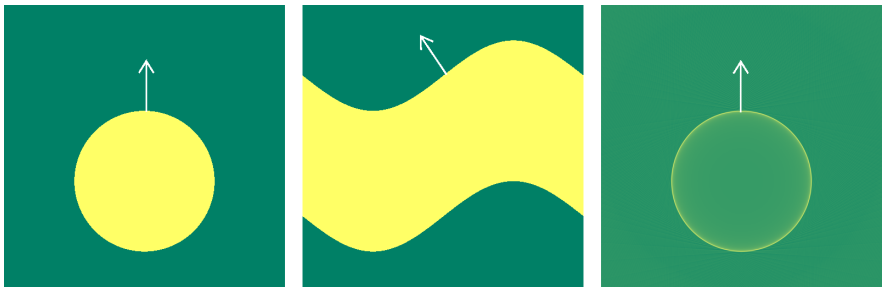

(a) (b) (c)

FIGURE 3. Imaging from the silhouettes of a disk K: (a) $f = \mathbb{1}_K$, (b) $g = \mathcal{S}[K]$, (c) $\mathcal{R}^*\Lambda g$.

3.2. **Imaging from silhouettes.** We consider the following imaging problem: reconstruct the scene K from the knowledge of the silhouettes $g(\theta, s) = \mathcal{S}[K](\theta, s), \theta \in [0, 2\pi], s \in \mathbb{R}$. It is known that the biggest set of $\mathbb{R}^2$ whose silhouette coincides with $\mathcal{S}[K]$ is $(\mathcal{R}^*\mathcal{S}[K])^{-1}(2\pi)$; it is called the visual hull of K [9]. Here we aim at testing the heuristic approach when the dataset g contains the silhouette $\mathcal{S}[K]$. For that purpose, we represent the compact K by the function $f = \mathbb{1}_K$. Due to the symmetry $\mathcal{S}[K](\theta, s) = -\mathcal{S}[K](\theta + \pi, -s)$, the singularities of $\mathrm{WF}\,\mathcal{S}[K]$ do not disappear: $D(g, f) = \emptyset$. We now investigate $\mathrm{WF}\,\mathcal{R}^*\mathcal{S}[K]$ for several canonical choices of K: a smooth convex set, a disjoint union of smooth convex sets, and a convex polygon. These are model problems where we have to deal with smooth sets, occlusions, corners and edges.

3.2.1. *Smooth convex set.* Let K be a smooth compact convex set. The singularities of $\mathbb{1}_K$ and of $\mathcal{R}\mathbb{1}_K$ are in correspondence with the tangents to ∂K:

$$\mathrm{WF}\,\mathbb{1}_K = \{(x, \sigma\boldsymbol{\theta}) : L(\theta, x \cdot \boldsymbol{\theta}) \text{ is tangent to } \partial K \text{ at } x \in \partial K, \theta \in [0, 2\pi], \sigma \neq 0\};$$

$$\mathrm{WF}\,\mathcal{R}[\mathbb{1}_K] = \{(\theta, x \cdot \boldsymbol{\theta}, -\sigma x \cdot \boldsymbol{\theta}^\perp, \sigma) : L(\theta, x \cdot \boldsymbol{\theta}) \text{ is tangent to } \partial K \text{ at } x \in \partial K, \theta \in [0, 2\pi], \sigma \neq 0\}.$$

We parametrize ∂K by the exterior normal vector $\boldsymbol{\theta}$: $\gamma(\theta), \theta \in [0, 2\pi]$. The tangents to ∂K are the lines $x \cdot \boldsymbol{\theta} = \gamma(\theta) \cdot \boldsymbol{\theta}$ and $x \cdot \boldsymbol{\theta} = \gamma(\theta + \pi) \cdot \boldsymbol{\theta}$. We see that $\mathcal{S}[K] = \mathbb{1}_A$, with $A = \{(\theta, s) : \gamma(\theta + \pi) \cdot \boldsymbol{\theta} \leqslant s \leqslant \gamma(\theta) \cdot \boldsymbol{\theta}\}$. The delimiting curves of A, $s = \gamma(\theta) \cdot \boldsymbol{\theta}$ and $s = \gamma(\theta + \pi) \cdot \boldsymbol{\theta}$, are smooth, with normal vectors $(-\dot\gamma(\theta) \cdot \boldsymbol{\theta} - \gamma(\theta) \cdot \boldsymbol{\theta}^\perp, 1) = (-\gamma(\theta) \cdot \boldsymbol{\theta}^\perp, 1)$ and $(-\gamma(\theta + \pi) \cdot \boldsymbol{\theta}^\perp, 1)$. Therefore, we get $\mathrm{WF}\,\mathcal{S}[K] = \mathrm{WF}\,\mathcal{R}[\mathbb{1}_K]$, and after backprojection, $C(\mathcal{S}[K], \mathbb{1}_K) = \mathrm{WF}\,\mathbb{1}_K = \mathrm{WF}\,\mathcal{R}^*\mathcal{S}[K]$. As a result, the wavefront set of $\mathbb{1}_K$ is perfectly recovered, and the reconstruction is artifact-free. See Figure 3, where the arrows represent elements of the wavefront sets.

3.2.2. *Disjoint union of convex sets.* Let $K = K_1 \cup K_2$, where K_1 and K_2 are disjoint smooth convex sets; $K_1 \cap K_2 = \emptyset$. The wavefront set of $\mathbb{1}_K$ is:

$$\mathrm{WF}\,\mathbb{1}_K = \{(x, \sigma\boldsymbol{\theta}) : L(\theta, x \cdot \boldsymbol{\theta}) \text{ is tangent to } \partial K \text{ at } x \in \partial K, \theta \in [0, 2\pi], \sigma \neq 0\}.$$

For the Radon transform, $\mathcal{R}[\mathbb{1}_K] = \mathcal{R}[\mathbb{1}_{K_1}] + \mathcal{R}[\mathbb{1}_{K_2}]$. Due to the canonical relation (15) and $K_1 \cap K_2 = \emptyset$, the sets $\mathrm{WF}\,\mathcal{R}[\mathbb{1}_{K_i}]$ are disjoint:

$$\mathrm{WF}\,\mathcal{R}[\mathbb{1}_{K_i}] = \{(\theta, x \cdot \boldsymbol{\theta}, -\sigma x \cdot \boldsymbol{\theta}^\perp, \sigma) : L(\theta, x \cdot \boldsymbol{\theta}) \text{ is tangent to } \partial K_i \text{ at } x \in \partial K_i, \theta \in [0, 2\pi], \sigma \neq 0\};$$

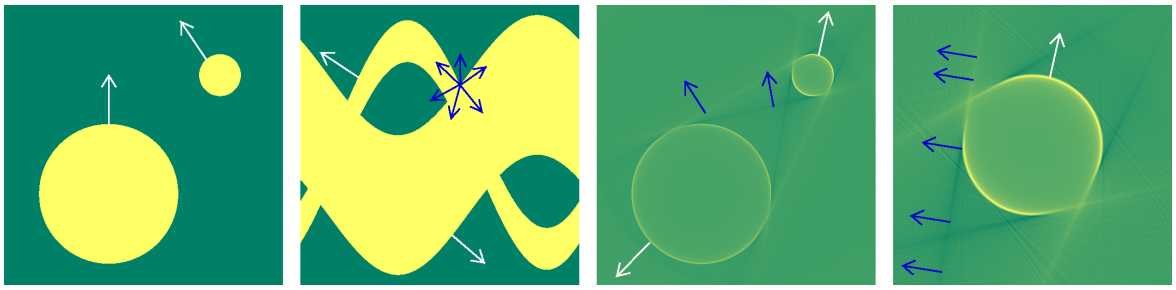

(a) (b) (c) (d)

FIGURE 4. Imaging from the silhouettes of two disks $K = K_1 \cup K_2$: (a) $f = \mathbb{1}_K$, (b) $g = \mathcal{S}[K]$, (c) $\mathcal{R}^*\Lambda g$, (d) zoom on $\mathcal{R}^*\Lambda g$.

so $\operatorname{WF}\mathcal{R}[\mathbb{1}_K] = \operatorname{WF}\mathcal{R}[\mathbb{1}_{K_1}] \cup \operatorname{WF}\mathcal{R}[\mathbb{1}_{K_2}]$. For the silhouettes, $\operatorname{WF}\mathcal{R}[\mathbb{1}_{K_i}] = \operatorname{WF}\mathcal{S}[K_i]$. The condition (8) is satisfied because $K_1 \cap K_2 = \emptyset$. And so we apply the inclusion (10) for $g = \mathcal{S}[K_1 \cup K_2]$; we get:

$$\check{C}(g,f) = \operatorname{WF}\mathcal{R}f \cap \{(\theta,s,\hat{\theta},\hat{s}) : L(\theta,s) \cap \operatorname{int} K = \emptyset\},$$
$$\check{A}(g,f) \subset \{(\theta,s) : L(\theta,s) \text{ is tangent to both } \partial K_1 \text{ and } \partial K_2\} \times (\mathbb{R}^2 \setminus \{0\}),$$
$$\check{I}(g,f) = \operatorname{WF}\mathcal{R}f \cap \{(\theta,s,\hat{\theta},\hat{s}) : L(\theta,s) \cap \operatorname{int} K \neq \emptyset\},$$
$$C(g,f) = \{(x,\sigma\boldsymbol{\theta}) : L(\theta, x\cdot\boldsymbol{\theta}) \text{ is tangent to } \partial K \text{ at } x \in \partial K \text{ and } L(\theta,x\cdot\boldsymbol{\theta}) \cap \operatorname{int} K = \emptyset, \theta \in [0,2\pi], \sigma \neq 0\},$$
$$A(g,f) \subset \{(x,\sigma\boldsymbol{\theta}) : L(\theta, x\cdot\boldsymbol{\theta}) \text{ is tangent to } \partial K \text{ at two points}, \theta \in [0,2\pi], \sigma \neq 0\},$$
$$I(g,f) = \{(x,\sigma\boldsymbol{\theta}) : L(\theta, x\cdot\boldsymbol{\theta}) \text{ is tangent to } \partial K \text{ at } x \in \partial K \text{ and } L(\theta,x\cdot\boldsymbol{\theta}) \cap \operatorname{int} K \neq \emptyset, \theta \in [0,2\pi], \sigma \neq 0\}.$$

The well-reconstructed parts in $\mathcal{R}^*\mathcal{S}[K]$ are the points $x \in \partial K$ where the tangent does not penetrate inside K. The points $x \in \partial K$ such that the tangent at x penetrates inside K are invisible. The artifacts are supported by the intermediate lines: the tangents to ∂K_1 and ∂K_2, associated with the corners of $\operatorname{supp} g$. See Figure 4, where the white arrows belong to the correct wavefront sets, $\operatorname{WF} f$, $\check{C}(g,f)$ and $C(g,f)$, while the blue arrows belong to the sets that estimate the artifact sets $\check{A}(g,f)$ and $A(g,f)$.

3.2.3. *Convex polygon.* Let K be a convex polygon, defined by the vertices $a_1,\dots,a_n \in \mathbb{R}^2$, such that the interior normal vector to the side $[a_{i-1},a_i]$ is $\boldsymbol{\theta}_i$, with $0 \leqslant \theta_1 < \theta_2 < \ldots < \theta_n < 2\pi$; $K = \{x : (x-a_i)\cdot\boldsymbol{\theta}_i \geqslant 0, 1 \leqslant i \leqslant n\}$. For convenience we extend the indexation by n-periodicity. The wavefront set of $\mathbb{1}_K$ is obtained from the sides and the corners:

$$\operatorname{WF}\mathbb{1}_K = \{(x,\sigma\boldsymbol{\theta}_i) : x \in (a_{i-1},a_i), \sigma \neq 0, 1 \leqslant i \leqslant n\} \cup \{(a_i,\hat{x}), \hat{x} \neq 0, 1 \leqslant i \leqslant n\}.$$

The corresponding wavefront set of $\mathcal{R}\mathbb{1}_K$ is:

$$\operatorname{WF}\mathcal{R}\mathbb{1}_K = \{(\theta, x\cdot\boldsymbol{\theta}, -\sigma x\cdot\boldsymbol{\theta}^\perp, \sigma) : x \in (a_{i-1},a_i), \theta = \theta_i(\pi), \sigma \neq 0, 1 \leqslant i \leqslant n\}$$
$$\cup \{(\theta, a_i\cdot\boldsymbol{\theta}, -\sigma a_i\cdot\boldsymbol{\theta}^\perp, \sigma), \theta \in [0,2\pi], \sigma \neq 0, 1 \leqslant i \leqslant n\}.$$

The singular support of the silhouette represents the lines that meet the vertices of K without penetrating inside K; it is a union of pieces of sinusoids:

$$\operatorname{supp sing}\mathcal{S}[K] = \{(\theta,s) : L(\theta,s) \cap \partial K \neq \emptyset \text{ and } L(\theta,s) \cap \operatorname{int} K = \emptyset\} = \{(\theta, a_i\cdot\boldsymbol{\theta}), \theta(\pi) \in [\theta_i,\theta_{i+1}], 1 \leqslant i \leqslant n\}.$$

If $(\theta, a_i\cdot\boldsymbol{\theta}) \in \operatorname{supp sing}\mathcal{S}[K]$ with $\theta(\pi) \in (\theta_i,\theta_{i+1})$, then it belongs to a single piece of sinusoid whose normal direction is $(-a_i\cdot\boldsymbol{\theta}^\perp, 1)$, so $\operatorname{WF}_{(\theta,a_i\cdot\boldsymbol{\theta})}\mathcal{S}[K] = \{(-\sigma a_i\cdot\boldsymbol{\theta}^\perp,\sigma), \sigma \neq 0\}$. If $(\theta, a_{i-1}\cdot\boldsymbol{\theta}) = (\theta, a_i\cdot\boldsymbol{\theta}) \in \operatorname{supp sing}\mathcal{S}[K]$ with $\theta(\pi) = \theta_i$, then it is the intersection of two pieces of sinusoids, whose normal directions are linearly independent: $(-a_{i-1}\cdot\boldsymbol{\theta}^\perp, 1)$ and $(-a_i\cdot\boldsymbol{\theta}^\perp, 1)$, and then $\operatorname{WF}_{(\theta,a_i\cdot\boldsymbol{\theta})}\mathcal{S}[K] = \mathbb{R}^2\setminus\{0\}$, with $\theta(\pi) = \theta_i$.

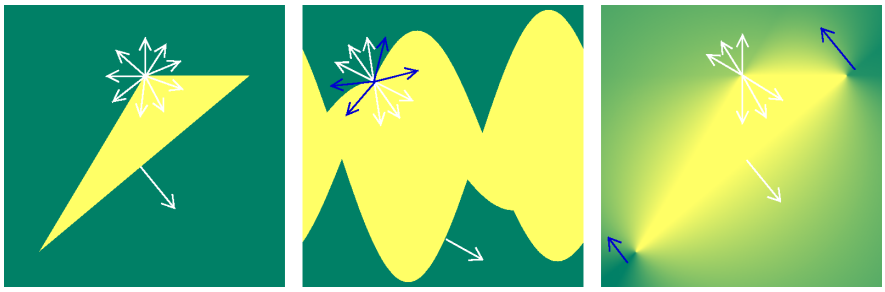

(a) (b) (c)

FIGURE 5. Imaging from the silhouettes of a triangle K: (a) $f = \mathbb{1}_K$, (b) $g = \mathcal{S}[K]$, (c) $\mathcal{R}^* g$.

Finally:

$$\begin{aligned}\operatorname{WF} \mathcal{S}[K] = \{(\theta, a_i \cdot \boldsymbol{\theta}, -\sigma a_i \cdot \boldsymbol{\theta}^\perp, \sigma) : \theta(\pi) \in (\theta_i, \theta_{i+1}), \sigma \neq 0, 1 \leqslant i \leqslant n\} \\ \cup \{(\theta, a_i \cdot \boldsymbol{\theta}), \theta(\pi) = \theta_i, 1 \leqslant i \leqslant n\} \times \mathbb{R}^2 \setminus \{0\}.\end{aligned}$$

We obtain:

$$\begin{aligned}\check{C}(g,f) &= \{(\theta, a_i \cdot \boldsymbol{\theta}, -\sigma a_i \cdot \boldsymbol{\theta}^\perp, \sigma) : \theta(\pi) \in (\theta_i, \theta_{i+1}), \sigma \neq 0, 1 \leqslant i \leqslant n\} \\ &\qquad \cup \{(\theta, x \cdot \boldsymbol{\theta}, -\sigma x \cdot \boldsymbol{\theta}^\perp, \sigma) : x \in [a_{i-1}, a_i], \theta = \theta_i(\pi), \sigma \neq 0, 1 \leqslant i \leqslant n\}, \\ \check{A}(g,f) &= \{(\theta, a_i \cdot \boldsymbol{\theta}), \theta(\pi) = \theta_i, 1 \leqslant i \leqslant n\} \times \mathbb{R}^2 \setminus \{0\} \\ &\qquad \setminus \{(\theta, a_i \cdot \boldsymbol{\theta}, -\sigma x \cdot \boldsymbol{\theta}^\perp, \sigma) : x \in [a_{i-1}, a_i], \theta = \theta_i(\pi), \sigma \neq 0, 1 \leqslant i \leqslant n\}, \\ \check{I}(g,f) &= \{(\theta, a_i \cdot \boldsymbol{\theta}, -\sigma a_i \cdot \boldsymbol{\theta}^\perp, \sigma), \theta(\pi) \notin [\theta_i, \theta_{i+1}], \sigma \neq 0, 1 \leqslant i \leqslant n\}, \\ C(g,f) &= \{(a_i, \sigma\boldsymbol{\theta}) : \theta(\pi) \in (\theta_i, \theta_{i+1}), \sigma \neq 0, 1 \leqslant i \leqslant n\} \cup \{(x, \sigma\boldsymbol{\theta}_i) : x \in [a_{i-1}, a_i], \sigma \neq 0, 1 \leqslant i \leqslant n\}, \\ A(g,f) &= \{(x, \sigma\boldsymbol{\theta}_i) : x \cdot \boldsymbol{\theta}_i = a_i \cdot \boldsymbol{\theta}_i, x \notin [a_{i-1}, a_i], \sigma \neq 0, 1 \leqslant i \leqslant n\}, \\ I(g,f) &= \{(a_i, \sigma\boldsymbol{\theta}) : \theta(\pi) \notin [\theta_i, \theta_{i+1}], \sigma \neq 0, 1 \leqslant i \leqslant n\}.\end{aligned}$$

The reconstruction $\mathcal{R}^*\mathcal{S}[K]$ contains the singularities of $\mathbb{1}_K$, except some ranges of directions at the vertices. In particular, the polygon ∂K is included in the singular support of the reconstruction. Moreover, the artifacts are supported by the lines containing the sides of the polygon (minus the sides themselves). See Figure 5.

3.3. **Truncation.** We model a simple case where the scene is not captured from all of the possible angles (limited angle), and where the scene is only partially projected when the angle is fixed (spatial truncation). Let $K = \{|x| \leqslant 1\}$ be the unit disk, represented by $f = \mathbb{1}_K$. We assume that we know the silhouettes $\mathcal{S}[K](\theta, s) = \mathbb{1}_{[-1,1]}(s), \theta \in [0, T], -2 \leqslant s \leqslant S$, with $T < \pi$ and $S < 1$. Alternatively, the measurements are a truncation of the full silhouette $g(\theta, s) = \mathcal{S}[K](\theta, s)\mathbb{1}_{0 \leqslant \theta \leqslant T, s \leqslant S}, \theta \in [0, 2\pi], s \in \mathbb{R}$. It can be checked that:

$$\begin{aligned}\check{C}(g,f) &= \{(\theta, -1, 0, \sigma) : \theta \in [0, T], \sigma \neq 0\} \\ \check{A}(g,f) &= \{(\theta, s, \sigma, 0) : \theta \in \{0, T\}, s \in (-1, S), \sigma \neq 0\} \\ &\qquad \cup \{(\theta, s, \hat{\theta}, \hat{s}) : \theta \in \{0, T\}, s \in \{-1, S\}, \hat{\theta} \neq 0\} \cup \{(\theta, S, 0, \sigma) : \theta \in [0, T], \sigma \neq 0\}, \\ \check{I}(g,f) &= \{(\theta, -1, 0, \sigma) : \theta \in (T, 2\pi), \sigma \neq 0\} \cup \{(\theta, 1, 0, \sigma) : \theta \in [0, 2\pi], \sigma \neq 0\} \\ C(g,f) &= \{(-\boldsymbol{\theta}, \sigma\boldsymbol{\theta}) : \theta \in [0, T], \sigma \neq 0\}, \\ A(g,f) &= \{(s\boldsymbol{\theta} + t\boldsymbol{\theta}^\perp, \sigma\boldsymbol{\theta}) : \theta \in \{0, T\}, s \in \{-1, S\}, t \neq 0, \sigma \neq 0\} \cup \{(S\boldsymbol{\theta}, \sigma\boldsymbol{\theta}) : \theta \in [0, T], \sigma \neq 0\}, \\ I(g,f) &= \{(-\boldsymbol{\theta}, \sigma\boldsymbol{\theta}) : \theta \in (T, 2\pi), \sigma \neq 0\}.\end{aligned}$$

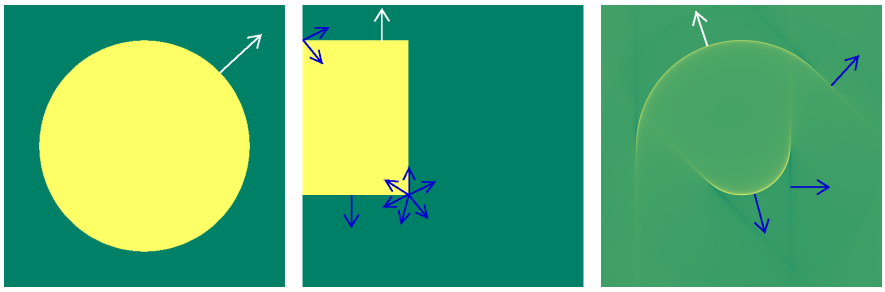

(a) (b) (c)

FIGURE 6. Imaging from incomplete silhouettes: (a) $f = \mathbb{1}_K$, (b) $g = \mathcal{S}[K]\mathbb{1}_{\mathbb{1}_{0\leqslant\theta\leqslant T, s\leqslant S}}$, (c) $\mathcal{R}^*\Lambda g$.

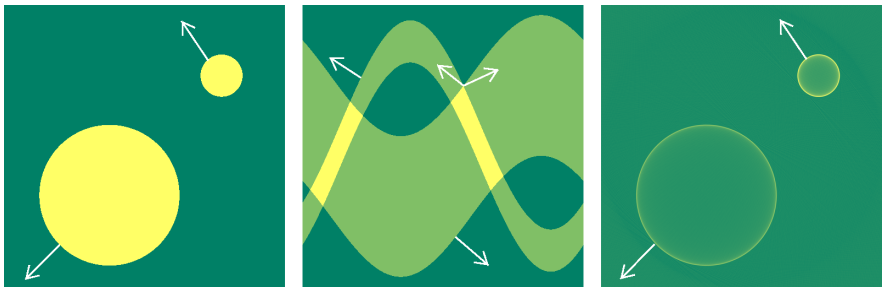

(a) (b) (c)

FIGURE 7. Imaging from the constructible Radon transform of two disks K_1, K_2: (a) $f = \mathbb{1}_{K_1} + \mathbb{1}_{K_2}$, (b) $g = \mathcal{S}[K_1] + \mathcal{S}[K_2]$, (c) $\mathcal{R}^*\Lambda g$.

The method recovers the portion of the circle that is visible along the singularities of the dataset. The spatial truncation introduce artifacts supported by a portion of circle, while the limited angle introduces the tangent straight lines at extremities. We get here the same kind of artifacts than the artifacts from a limited Radon transform in usual tomography: the same reasons produce the same effects. See Figure 6.

3.4. **Euler-Poincaré index.** We apply the heuristic in a framework of constructible tomography. Let $K = K_1 \cup K_2$, where K_1 and K_2 are two disjoint disks. The constructible function $f = \mathbb{1}_{K_1} + \mathbb{1}_{K_2}$ represents K. We define g as the constructible Radon transform of f: for every $\theta \in [0, 2\pi], s \in \mathbb{R}$, $g(\theta, s)$ is the number of connected components of $L(\theta, s) \cap K$. We see, from the paragraph 3.1.1 about the sum of silhouettes, that $g = \mathcal{S}[K_1] + \mathcal{S}[K_2]$. Thus $\mathrm{WF}\, g = \mathrm{WF}\, \mathcal{R} f = \mathrm{WF}\, \mathcal{R}[\mathbb{1}_{K_1}] \cup \mathrm{WF}\, \mathcal{R}[\mathbb{1}_{K_2}]$ (disjoint union), and so $C(g, f) = \mathrm{WF}\, \mathcal{R}^* g = \mathrm{WF}\, f$. On this example, the dual of the usual Radon transform recovers exactly the singularities of a constructible function, from its constructible Radon transform. See Figure 7.

3.5. **Cloaking and counter-cloaking.** We illustrate on a simple example a property of cloaking, due to disappearances. Let $K = \{|x| \leqslant 1\}$. We assume that we have measured: $g(\theta, s) = 3 + (s + \frac{1}{2}\cos(\theta))\mathbb{1}_{-1\leqslant s\leqslant 1}, \theta \in [0, 2\pi], s \in \mathbb{R}$. With $f = \mathbb{1}_K$, $\mathrm{WF}\, g = \mathrm{WF}\, \mathcal{R} f$, and thus $C(g, f) = \mathrm{WF}\, f$. Here, g_{sym} is smooth; we get from Proposition 3(ii) that $D(g, f) = C(g, f)$ and $\mathrm{WF}\, \mathcal{R}^* g = \emptyset$! We see here that the wavefront set of g is perfect, but the anti-symmetry property completely cancels the singularities during the backprojection.

This effect can be corrected. For example, we multiply g by a function that kills the anti-symmetry, without changing the wavefront set: we compute $\mathcal{R}^*\tilde{g}$, with $\tilde{g}(\theta, s) = (s + \frac{1}{2}\sin(\theta))g(\theta, s)$. The symmetric part of $\tilde{g}$ is $\tilde{g}_{\mathrm{sym}}(\theta, s) = (s + \frac{1}{2}\sin(\theta))(s + \frac{1}{2}\cos(\theta))\mathbb{1}_{-1\leqslant s\leqslant 1}, \theta \in [0, 2\pi], s \in \mathbb{R}$. We apply now Proposition 3(i): $D(\tilde{g}_{\mathrm{sym}}, f) = \emptyset$, and then $\mathrm{WF}\, \mathcal{R}^*\tilde{g} = \mathrm{WF}\, f$; this is now perfect. See Figure 8.

3.6. **Cartoon images.** We test the heuristic method on cartoon images with occlusions and contrasts. We assume that the smooth convex set K_1 is projected with constant value $f_1 > 0$, while a second smooth convex

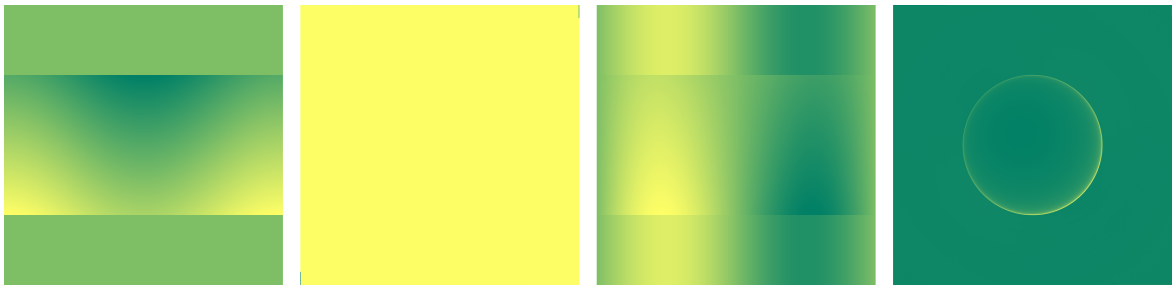

(a) (b) (c) (d)

FIGURE 8. Cloaking and counter-cloaking: (a) g is "anti-symmetric", (b) $\mathcal{R}^*\Lambda g$ sees nothing, (c) $\tilde{g}(\theta,s) = (s + \frac{1}{2}\sin(\theta))g(\theta,s)$ breaks the anti-symmetry, (d) $\mathcal{R}^*\Lambda\tilde{g}$ sees the initial disk.

set K_2, well-separated from K_1, is projected with constant value $f_2 > 0$. The scene $K = K_1 \cup K_2$ can be represented by $f = f_1\mathbb{1}_{K_1} + f_2\mathbb{1}_{K_2}$, such that $\mathrm{WF}\,\mathcal{R}f = \mathrm{WF}\,\mathcal{R}\mathbb{1}_{K_1} \cup \mathrm{WF}\,\mathcal{R}\mathbb{1}_{K_2}$ (disjoint union). For every ray $(\theta,s) \in [0,2\pi]\times\mathbb{R}$, if $L(\theta,s)\cap K = \emptyset$, then we set $g(\theta,s) = 0$. Otherwise, we set $g(\theta,s) = f(x) \in \{f_1,f_2\}$, where $x \in \partial K$ minimizes $x\cdot\boldsymbol{\theta}^\perp$ over the set $L(\theta,s)\cap K$. We assume that the images are contrasted: $f_1 \neq f_2$. Otherwise g would contain exactly the silhouettes of K, discussed previously. We notice that if $L(\theta,s)\cap K_1 \neq 0$ and $L(\theta,s)\cap K_2 \neq 0$, then one of the disks is occluded. We have the following decomposition: $g = f_1\mathcal{S}[K_1]+f_2\mathcal{S}[K_2]-f_1\mathbb{1}_{K_2 \text{ conceals } K_1}-f_2\mathbb{1}_{K_1 \text{ conceals } K_2}$. The symmetric part g_{sym} of g can be decomposed using the silhouettes and the symmetric concealment function $\mathcal{S}[K_1]\mathcal{S}[K_2]$:

$$g_{\mathrm{sym}}(\theta,s) = f_1\mathcal{S}[K_1] + f_2\mathcal{S}[K_2] - \frac{f_1+f_2}{2}\mathcal{S}[K_1]\mathcal{S}[K_2].$$

We deduce from $\mathrm{WF}\,\mathcal{R}\mathbb{1}_{K_i} = \mathrm{WF}\,\mathcal{S}[K_i]$ and $f_1 \neq f_2$:

$$\{(\theta,s,\hat{\theta},\hat{s}) \in \mathrm{WF}\,\mathcal{R}\mathbb{1}_{K_i} : (\theta,s) \notin \operatorname{supp}\operatorname{sing}\mathcal{R}\mathbb{1}_{K_i}, i=1,2\}$$
$$\subset \mathrm{WF}\,g_{\mathrm{sym}} \subset \mathrm{WF}\,\mathcal{R}\mathbb{1}_{K_1} \cup \mathrm{WF}\,\mathcal{R}\mathbb{1}_{K_2} \cup \mathrm{WF}\,\mathcal{S}[K_1]\mathcal{S}[K_2].$$

Passing to the closure for the left-hand side:

$$\mathrm{WF}\,\mathcal{R}f \subset \mathrm{WF}\,g_{\mathrm{sym}} \subset \mathrm{WF}\,\mathcal{R}f \cup \mathrm{WF}\,\mathcal{S}[K_1]\mathcal{S}[K_2]. \tag{11}$$

The first inclusion of (11) guarantees that

$$\check{C}(g_{\mathrm{sym}},f) = \mathrm{WF}\,\mathcal{R}f, \quad C(g,f) = C(g_{\mathrm{sym}},f) = \mathrm{WF}\,f,$$

and so the whole geometry is recovered. In comparison with the reconstruction from silhouettes, the set of singularities of g is augmented due to the contrast $f_1 \neq f_2$. As a result we recover more information: the invisible part is now empty. By the way $K_1 \cap K_2 = \emptyset$, so (8) is true and (9) estimates the singularities due to the concealment:

$$\mathrm{WF}\,\mathcal{S}[K_1]\mathcal{S}[K_2] \subset \{(\theta,s,\hat{\theta}_1+\hat{\theta}_2,\hat{s}_1+\hat{s}_2) : (\theta,s,\hat{\theta}_i,\hat{s}_i) \in \mathrm{WF}\,\mathcal{S}[K_i] \cup \operatorname{supp}\mathcal{S}[K_i]\times\{0\}, i=1,2\}.$$

We get from the second inclusion of (11):

$$\check{A}(g,f) = \check{A}(g_{\mathrm{sym}},f) \subset \{(\theta,s,\hat{\theta}_1+\hat{\theta}_2,\hat{s}_1+\hat{s}_2) : (\theta,s,\hat{\theta}_i,\hat{s}_i) \in \mathrm{WF}\,\mathcal{S}[K_i], i=1,2\}$$
$$\subset \operatorname{supp}\operatorname{sing}\mathcal{R}\mathbb{1}_{K_1} \cap \operatorname{supp}\operatorname{sing}\mathcal{R}\mathbb{1}_{K_2} \times \mathbb{R}^2 \setminus \{0\},$$

$$A(g,f) = A(g_{\mathrm{sym}},f) \subset \{(x,\sigma\boldsymbol{\theta}) : L(\theta,x\cdot\boldsymbol{\theta}) \text{ is tangent to } \partial K \text{ at two points}, \sigma \neq 0\}.$$

The artifacts due to concealment are supported by the common tangents of ∂K_1 and ∂K_2, as for the union of silhouettes. See Figure 9.

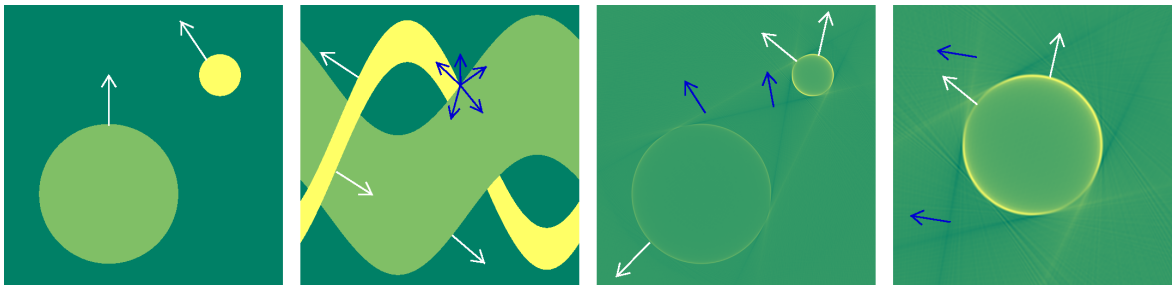

(a) (b) (c) (d)

FIGURE 9. Imaging from cartoon images of two disks K_1, K_2: (a) $f = f_1 \mathbb{1}_{K_1} + f_2 \mathbb{1}_{K_2}$, (b) g, (c) $\mathcal{R}^*\Lambda g$, (d) zoom on $\mathcal{R}^*\Lambda g$.

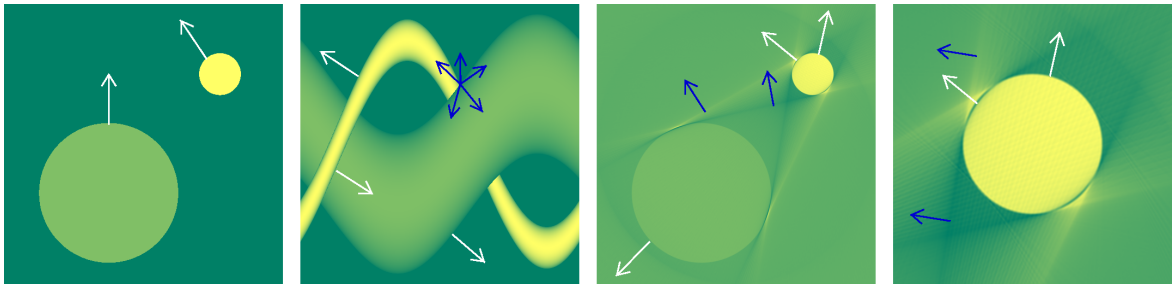

(a) (b) (c) (d)

FIGURE 10. Reflective tomography of two lambertian disks K_1, K_2: (a) $f = f_1 \mathbb{1}_{K_1} + f_2 \mathbb{1}_{K_2}$, (b) $g = f(v)\boldsymbol{\theta}^\perp \cdot \nu$, (c) $\mathcal{R}^*\Lambda g$, (d) zoom on $\mathcal{R}^*\Lambda g$.

3.7. **Lambertian diffusion.** We model a case of reflective tomography. We want to reconstruct the boundary ∂K of a compact K using an active imaging system as follows. The acquisition device turns around the scene K: for the angle θ, it is located at $-\rho\boldsymbol{\theta}^\perp$, where ρ is very large compared with the size of K. It illuminates the scene with a light source, and records the intensity $g(\theta, \cdot)$ of the light reflected off the objects, on a focal plane directed by $\boldsymbol{\theta}$. We describe below a lambertian model of g for $K = K_1 \cup K_2$, where K_1 and K_2 are two disjoint disks (centers z_i, radii r_i).

We assume that the objects K_1 and K_2 have a constant albedo: $f_1 > 0$ and $f_2 > 0$. So we set $f = f_1 \mathbb{1}_{K_1} + f_2 \mathbb{1}_{K_2}$. For $\theta \in [0, 2\pi], s \in \mathbb{R}$, if the ray $L(\theta, s)$ does not meet K, then $g(\theta, s) = 0$. Otherwise, the device sees the visible point $v(\theta, s) \in \partial K$, that minimizes $x \cdot \boldsymbol{\theta}^\perp$ over the set $L(\theta, s) \cap K$. The interior unit normal of K at $v(\theta, s)$ is denoted by $\nu(\theta, s)$. The Lambert's cosine law that we assume is the following:

$$g(\theta, s) = f(v(\theta, s))\boldsymbol{\theta}^\perp \cdot \nu(\theta, s).$$

So $g(\theta, s) = \tilde{g}(\theta, s)\boldsymbol{\theta}^\perp \cdot \nu(\theta, s)$, where $\tilde{g}$ is the cartoon image of the albedo f, while $\boldsymbol{\theta}^\perp \cdot \nu(\theta, s)$ is a smooth function on the pieces where $\tilde{g}$ is constant: if $v(\theta, s) \in K_i$, then $\nu(\theta, s) = -\frac{s - z_i \cdot \boldsymbol{\theta}}{r_i}\boldsymbol{\theta} + \sqrt{1 - (\frac{s - z_i \cdot \boldsymbol{\theta}}{r_i})^2}\boldsymbol{\theta}^\perp$. And thus $\mathrm{WF}\, g \subset \mathrm{WF}\, \tilde{g}$, and $\mathrm{WF}\, \mathcal{R}^* g \subset \mathrm{WF}\, \mathcal{R}^* \tilde{g}$: we expect the heuristic to recover the same singularities with the lambertian model and with the cartoon model, with the same kind of artifacts. See Figure 10.

APPENDIX A. MICROLOCAL ANALYSIS OF THE BACKPROJECTION

We summarize microlocal properties of the Radon transform. See [3] for detailed descriptions.

A.1. **Radon transform.** The Radon transform $\mathcal{R}$ maps a function $f \in L^2(\mathbb{R}^2)$ onto $\mathcal{R}[f]$ defined by:

$$\mathcal{R}[f](\theta, s) = \int f(x)\delta(x \cdot \boldsymbol{\theta} - s)\mathrm{d}x = \int_{L(\theta,s)} f(x)\mathrm{d}\sigma, \quad \theta \in [0, 2\pi], s \in \mathbb{R}, \tag{12}$$

where $L(\theta, s) = \{x : x \cdot \boldsymbol{\theta} = s\} = \{s\boldsymbol{\theta} + t\boldsymbol{\theta}^\perp, t \in \mathbb{R}\}$ is the line normal to $\boldsymbol{\theta} = (\cos\theta, \sin\theta)$, directed by $\boldsymbol{\theta}^\perp = (-\sin\theta, \cos\theta)$, and at signed distance s from the origin. So $\mathcal{R}[f](\theta, s)$ integrates f along the line $x \cdot \boldsymbol{\theta} - s = 0$, where (θ, s) is fixed. The dual operator $\mathcal{R}^*$ of $\mathcal{R}$ is called the backprojection. It maps a function $g \in L^1_{\mathrm{loc}}([0, 2\pi] \times \mathbb{R})$ (2π-periodic with respect to the first place) onto $\mathcal{R}^*[g]$ such that:

$$\mathcal{R}^*[g](x) = \int_0^{2\pi} g(\theta, x \cdot \boldsymbol{\theta})\mathrm{d}\theta, \quad x = (x_1, x_2) \in \mathbb{R}^2. \tag{13}$$

Thus, $\mathcal{R}^*[g](x)$ integrates g along the sinusoid $x \cdot \boldsymbol{\theta} - s = 0$, where $x \in \mathbb{R}^2$ is fixed.

A.2. **Fourier integral operators.** The Radon transform $\mathcal{R}$ is an elliptic Fourier integral operator, with amplitude $\frac{1}{2\pi}$ and phase $\psi(\theta, s, x, \sigma) = \sigma(s - \boldsymbol{\theta} \cdot x)$:

$$\mathcal{R}[f](\theta, s) = \int_{\mathbb{R}^2} \int_{\mathbb{R}} \frac{1}{2\pi} \mathrm{e}^{\mathrm{i}\sigma(s - \boldsymbol{\theta}\cdot x)} \mathrm{d}\sigma\, f(x)\mathrm{d}x, \quad f \in L^2(\mathbb{R}^2). \tag{14}$$

The canonical relation of $\mathcal{R}$ is:

$$\begin{aligned}\mathrm{WF}(\mathcal{R}[f]) = \big\{(\theta, s, \hat\theta, \hat s) \in T^*([0, 2\pi] \times \mathbb{R}) : \exists (x, \hat x) \in \mathrm{WF}(f), \exists \sigma \in \mathbb{R} \setminus \{0\}, \\ \partial_\sigma \psi = s - x \cdot \boldsymbol{\theta} = 0, \quad (\hat\theta, \hat s) = \partial_{(\theta,s)}\psi = \sigma(-x \cdot \boldsymbol{\theta}^\perp, 1), \quad \hat x = -\partial_x \psi = \sigma\boldsymbol{\theta}\big\}.\end{aligned} \tag{15}$$

This equality establishes a correspondence between the singularities of $\mathcal{R}f$ and f. As a consequence:

$$\begin{aligned}\mathrm{WF}(f) = \big\{(x, \hat x) \in T^*(\mathbb{R}^2) : \exists (\theta, s, \hat\theta, \hat s) \in \mathrm{WF}(\mathcal{R}f), \exists \sigma \in \mathbb{R} \setminus \{0\}, \\ s - x \cdot \boldsymbol{\theta} = 0, (\hat\theta, \hat s) = \sigma(-x \cdot \boldsymbol{\theta}^\perp, 1), \hat x = \sigma\boldsymbol{\theta}\big\}.\end{aligned} \tag{16}$$

The backprojection $\mathcal{R}^*$ is an elliptic Fourier integral operator, with amplitude $\frac{1}{2\pi}$ and phase $\varphi(x, \theta, s, \sigma) = \sigma(x \cdot \boldsymbol{\theta} - s)$:

$$\mathcal{R}^*[g](x) = \int_{[0,2\pi]\times\mathbb{R}} \int_{\mathbb{R}} \frac{1}{2\pi} \mathrm{e}^{\mathrm{i}\sigma(x\cdot\boldsymbol{\theta} - s)} \mathrm{d}\sigma\, g(\theta, s)\mathrm{d}\theta\mathrm{d}s, \quad g \in L^1_{\mathrm{loc}}([0, 2\pi] \times \mathbb{R}). \tag{17}$$

The canonical relation of $\mathcal{R}^*$ is:

$$\begin{aligned}\mathrm{WF}(\mathcal{R}^*[g]) \subset \big\{(x, \hat x) \in T^*\mathbb{R}^2 : \exists (\theta, s, \hat\theta, \hat s) \in \mathrm{WF}(g), \exists \sigma \in \mathbb{R} \setminus \{0\}, \\ \partial_\sigma \varphi = x \cdot \boldsymbol{\theta} - s = 0, \quad \hat x = \partial_x \varphi = \sigma\boldsymbol{\theta}, \quad (\hat\theta, \hat s) = -\partial_{(\theta,s)}\varphi = \sigma(-x \cdot \boldsymbol{\theta}^\perp, 1)\big\}.\end{aligned} \tag{18}$$

Furthermore, under the symmetry constraint $g(\theta + \pi, -s) = g(\theta, s)$, then the canonical relation (18) is an equality.

Remark 1. We set

$$\Phi(x, \hat x, \theta, s, \hat\theta, \hat s, \sigma) := (x \cdot \boldsymbol{\theta} - s, \hat x - \sigma\boldsymbol{\theta}, \hat\theta + \sigma x \cdot \boldsymbol{\theta}^\perp, \hat s - \sigma). \tag{19}$$

Then the canonical relations of $\mathcal{R}$ and $\mathcal{R}^*$ are expressed by the means of the equation: $\Phi(x, \hat x, \theta, s, \hat\theta, \hat s, \sigma) = 0$.

A.3. **Filtered backprojection.** If Λ is a pseudodifferential operator, then the filtered backprojection $\mathcal{R}^*\Lambda$ satisfies [15]:

$$\mathrm{WF}(\mathcal{R}^*\Lambda g) \subset \mathrm{WF}(\mathcal{R}^* g). \tag{20}$$

In particular, this is true for the filter that achieves the Radon inversion, $\Lambda = \frac{1}{4\pi}\sqrt{-\partial_s^2}$, and for the local filter of the so-called Λ-tomography, $\Lambda = -\partial_s^2$. Due to this inclusion, we restrict our attention to the study of $\mathrm{WF}(\mathcal{R}^* g)$.

Acknowledgments

The authors would like to thank Gilles Lebeau for his deep comments and fruitful discussions.

References

[1] G. Berginc and M. Jouffroy. Optronic system and method dedicated to identification for formulating three-dimensional images. US patent 20110254924 A1, European patent 2333481 A1, FR 09 05720 B1, November 2009.
[2] G. Berginc and M. Jouffroy. 3D laser imaging. *PIERS Online*, 7(5):411–415, 2011.
[3] L. Borg, J. Frikel, J.S. Jørgensen, and E.T. Quinto. Analyzing Reconstruction Artifacts from Arbitrary Incomplete X-ray CT Data. *SIAM Journal on Imaging Sciences*, 11(4):2786–2814, 2018.
[4] A. Faridani, E.L. Ritman, and K.T. Smith. Local tomography. *SIAM Journal on Applied Mathematics*, 52(2):459–484, 1992.
[5] J. Frikel and E.T. Quinto. Characterization and reduction of artifacts in limited angle tomography. *Inverse Problems*, 29(12):125007, 2013.
[6] D.T. Gering and W.M. Wells. Object modeling using tomography and photography. In *Multi-View Modeling and Analysis of Visual Scenes, 1999.(MVIEW'99) Proceedings. IEEE Workshop on*, pages 11–18. IEEE, 1999.
[7] A. Grigis and J. Sjöstrand. *Microlocal analysis for differential operators: an introduction*, volume 196. Cambridge University Press, 1994.
[8] F.K. Knight, S.R. Kulkarni, R.M. Marino, and J.K. Parker. Tomographic Techniques Applied to Laser Radar Reflective Measurements. *Lincoln Laboratory Journal*, 2(2):143–160, 1989.
[9] A. Laurentini. The visual hull concept for silhouette-based image understanding. *IEEE Transactions on pattern analysis and machine intelligence*, 16(2):150–162, 1994.
[10] F. Natterer and F. Wübbeling. *Mathematical methods in image reconstruction*. SIAM, 2001.
[11] E.T. Quinto. Singularities of the X-ray transform and limited data tomography in R^2 and R^3. *SIAM Journal on Mathematical Analysis*, 24(5):1215–1225, 1993.
[12] A.G. Ramm and A.I. Katsevich. *The Radon transform and local tomography*. CRC press, 1996.
[13] G. Rigaud, J.-B. Bellet, G. Berginc, I. Berechet, and S. Berechet. Reflective Imaging Solved by the Radon Transform. *IEEE Geoscience and Remote Sensing Letters*, 13:936–938, 2016.
[14] P. Schapira. Tomography of constructible functions. In *International Symposium on Applied Algebra, Algebraic Algorithms, and Error-Correcting Codes*, pages 427–435. Springer, 1995.
[15] P. Stefanov. *Microlocal Analysis Methods*, pages 914–920. Springer Berlin Heidelberg, Berlin, Heidelberg, 2015.

Université de Lorraine, CNRS, IECL, F-57000 Metz, France
E-mail address: jean-baptiste.bellet@univ-lorraine.fr

Thales Optronique, 2 avenue Gay Lussac, CS 90502, 78995 Élancourt Cedex, France
E-mail address: gerard.berginc@fr.thalesgroup.com